Biogeosciences, 15, 3331–3343, 2018
https://doi.org/10.5194/bg-15-3331-2018


Biogeosciences
Open Access
EGU

# $CO_2$ flux over young and snow-covered Arctic pack ice in winter and spring

**Daiki Nomura[1,2,3,4], Mats A. Granskog[5], Agneta Fransson[5], Melissa Chierici[6,7], Anna Silyakova[8], Kay I. Ohshima[1,3], Lana Cohen[5], Bruno Delille[9], Stephen R. Hudson[5], and Gerhard S. Dieckmann[10]**

[1]Institute of Low Temperature Science, Hokkaido University, Kita 19, Nishi 8, Kita-ku, Sapporo, Hokkaido 060-0819, Japan
[2]Faculty of Fisheries Sciences, Hokkaido University, 3-1-1, Minato-cho, Hakodate, Hokkaido 041-8611, Japan
[3]Arctic Research Center, Hokkaido University, Kita 21, Nishi 11, Kita-ku, Sapporo, Hokkaido 001-0021, Japan
[4]Global Station for Arctic Research, Global Institution for Collaborative Research and Education, Hokkaido University, Kita 8, Nishi 5, Kita-ku, Sapporo, Hokkaido 060-0808, Japan
[5]Norwegian Polar Institute, Fram Centre, 9296 Tromsø, Norway
[6]Institute of Marine Research, 9294, Tromsø, Norway
[7]FRAM-High North Research Centre for Climate and the Environment, Tromsø, Norway
[8]CAGE, Centre for Arctic Gas Hydrate, Environment and Climate, Tromsø, Norway
[9]Unité d'Océanographie Chimique, Freshwater and Oceanic Science Unit of Research (FOCUS), Université de Liège, Liège, Belgium
[10]Alfred Wegener Institute for Polar and Marine Research, Bremerhaven, Germany

**Correspondence:** Daiki Nomura (daiki.nomura@fish.hokudai.ac.jp)

Received: 5 December 2017 – Discussion started: 8 January 2018
Revised: 14 May 2018 – Accepted: 19 May 2018 – Published: 5 June 2018

**Abstract.** Rare $CO_2$ flux measurements from Arctic pack ice show that two types of ice contribute to the release of $CO_2$ from the ice to the atmosphere during winter and spring: young, thin ice with a thin layer of snow and older (several weeks), thicker ice with thick snow cover. Young, thin sea ice is characterized by high salinity and high porosity, and snow-covered thick ice remains relatively warm ($> -7.5\,^{\circ}C$) due to the insulating snow cover despite air temperatures as low as $-40\,^{\circ}C$. Therefore, brine volume fractions of these two ice types are high enough to provide favorable conditions for gas exchange between sea ice and the atmosphere even in mid-winter. Although the potential $CO_2$ flux from sea ice decreased due to the presence of the snow, the snow surface is still a $CO_2$ source to the atmosphere for low snow density and thin snow conditions. We found that young sea ice that is formed in leads without snow cover produces $CO_2$ fluxes an order of magnitude higher than those in snow-covered older ice ($+1.0 \pm 0.6\,mmol\,C\,m^{-2}\,day^{-1}$ for young ice and $+0.2 \pm 0.2\,mmol\,C\,m^{-2}\,day^{-1}$ for older ice).

## 1 Introduction

Arctic sea ice is changing dramatically, with rapid declines in summer sea ice extent and a shift towards younger and thinner first-year ice rather than thick multi-year ice (e.g., Stroeve et al., 2012; Meier et al., 2014; Lindsay and Schweiger, 2015). Although the effects of sea ice formation and melting on biogeochemical cycles in the ocean have previously been discussed (e.g., Vancoppenolle et al., 2013), the effects of sea ice freeze and melt processes on carbon dioxide ($CO_2$) exchange with the atmosphere are still largely unknown (Parmentier et al., 2013).

Recent $CO_2$ flux measurements on sea ice indicate that sea ice is an active component in gas exchange between ocean and atmosphere (Nomura et al., 2013; Geilfus et al., 2013, 2014; Delille et al., 2014; Brown et al., 2015; Kotovitch et al., 2016). The sea ice $CO_2$ fluxes depend on (a) the difference in the partial pressure of $CO_2$ ($pCO_2$) between the sea ice surface and air, (b) brine volume fraction at the ice–snow interface, (c) ice surface condition including the snow deposited on ice, and (d) wind-driven pressure pumping through the

snow. For (a), it is known that the air–sea ice $CO_2$ flux is driven by the differences in $pCO_2$ between the sea ice surface and atmosphere (e.g., Delille et al., 2014; Geilfus et al., 2014). Brine $pCO_2$ changes due to processes within the sea ice, such as thermodynamic process (e.g., Delille et al., 2014), biological activity (e.g., Delille et al., 2007; Fransson et al., 2013; Rysgaard et al., 2013), and calcium carbonate ($CaCO_3$; ikaite) formation and dissolution (e.g., Papadimitriou et al., 2012). When $pCO_2$ in brine is higher than that of air $pCO_2$, brine has the potential to release $CO_2$ to the atmosphere. Brine volume fraction (b) controls the permeability of sea ice (Golden et al., 1998) and thus $CO_2$ fluxes (Delille et al., 2014; Geilfus et al., 2014). The air–sea ice $CO_2$ flux is also strongly dependent on the sea ice surface conditions (c) (Nomura et al., 2010a, 2013; Geilfus et al., 2013, 2014; Barber et al., 2014; Brown et al., 2015; Fransson et al., 2015). Nomura et al. (2013) proposed that snow properties (e.g., water equivalent) are important factors affecting gas exchange processes on sea ice. In addition, frost flowers (vapor-deposited ice crystals that wick brine from the sea ice surface) promote $CO_2$ flux from the ice to the atmosphere (Geilfus et al., 2013; Barber et al., 2014; Fransson et al., 2015). Finally, for (d), it is thought that $CO_2$ flux is affected by wind pumping through the snow pack (Massman et al., 1995; Takagi et al., 2005) in which the magnitude of $CO_2$ flux through snow or underlying soil (e.g., Takagi et al., 2005) can increase the transport relative to molecular diffusion by up to 40 % (Bowling and Massman, 2011). These results were mainly found over land-based snow (soil and forest), and thus they are still poorly understood over sea ice (Papakyriakou and Miller, 2011).

In addition to the processes described above, the $CO_2$ flux over sea ice may also be influenced by the temperature difference between the ice surface and the atmosphere. This has been shown in previous studies in dry snowpacks over land surfaces. These studies show that there is an unstable air density gradient due to heating at the bottom producing a strong temperature difference between the bottom and top of the snowpack (e.g., Powers et al., 1985; Severinghaus et al., 2010). This produces air flow within the snowpack, which is a potentially significant contributor to mixing and transport of gas and heat within the snowpack. We expect that this process would also occur in snow over sea ice, especially during the wintertime when air temperatures are coldest and the temperature difference between sea ice surface (snow bottom) and atmosphere is largest (e.g., Massom et al., 2001). Generally, the sea ice surface under thick snow cover is warm due to the heat conduction from the bottom of sea ice and the insulating effect of the snow cover, and a strong temperature difference between the sea ice surface and atmosphere is observed (e.g., Massom et al., 2001). Such a temperature difference would produce an unstable air density gradient and upward transport of air containing $CO_2$ degassed at the sea ice surface, thereby enhancing $CO_2$ exchange between sea ice and atmosphere.

In the ice-covered Arctic Ocean, storm periods which produce high wind speeds and open leads are also important for air-to-sea $CO_2$ fluxes (Fransson et al., 2017) due to the undersaturation of the surface waters in $CO_2$ with respect to the atmosphere. In addition, the subsequent ice growth and frost flower formation in open leads promote ice-to-air $CO_2$ fluxes in winter (e.g., Barber et al., 2014). Given the fact that Arctic sea ice is shrinking and shifting from multi-year ice to first-year ice (e.g., Stroeve et al., 2012; Meier et al., 2014; Lindsay and Schweiger, 2015), the area of open ocean and thinner seasonal ice is increasing. Thus, a potential consequence may be increased contribution of open ocean surface and/or thinner sea ice to the overall $CO_2$ fluxes of the Arctic Ocean. The dynamics of the thinner ice pack, through formation of leads and new ice, will play an important role in the gas fluxes from the ice pack. However, there is a definite lack of information on sea ice processes during wintertime due to the difficulty in acquiring observations in winter pack ice, as reflected by the fact that most of the previous winter $CO_2$ flux measurements have been take over landfast ice.

The Norwegian young sea ICE (N-ICE2015) campaign in winter and spring 2015 provided opportunities to examine $CO_2$ fluxes between sea ice and atmosphere in a variety of snow and ice conditions in pack ice north of Svalbard. Formation of leads and their rapid refreezing allowed us to examine air–sea ice $CO_2$ fluxes over thin young sea ice, occasionally covered with frost flowers in addition to the snow-covered older ice that covers most of the pack ice area. The objectives of this study were to understand the effects of (i) thin sea ice and frost flower formation on the air–sea ice $CO_2$ flux in leads, (ii) effect of snow-cover on the air–sea ice $CO_2$ flux over thin, young ice in the Arctic Ocean during winter and spring seasons, and (iii) of the effect of the temperature difference between sea ice and atmosphere (including snow cover) on the air–sea ice $CO_2$ flux.

## 2 Materials and methods

### 2.1 Study area

This study was performed during N-ICE2015 campaign with R/V *Lance* in the pack ice north of Svalbard from January to June 2015 (Granskog et al., 2016). Air–sea ice $CO_2$ flux measurements were carried out from January to May 2015 during the drift of floes 1, 2, and 3 of the N-ICE2015 campaign (Figs. 1 and 2, Table 1). The ice pack was a mixture of young ice, first-year ice, and second-year ice (Granskog et al., 2017), and both the first- and second-year ice had a thick snow cover (Merkouriadi et al., 2017; Rösel et al., 2018). Air–sea ice $CO_2$ flux measurements were made over young ice (YI stations), first-year ice (FI stations), and old ice (multi-year ice) (OI station). In the N-ICE2015 study region, the modal ice thickness was about 1.3–1.5 m and the modal snow thickness was about 0.5 m (Rösel et al., 2018).

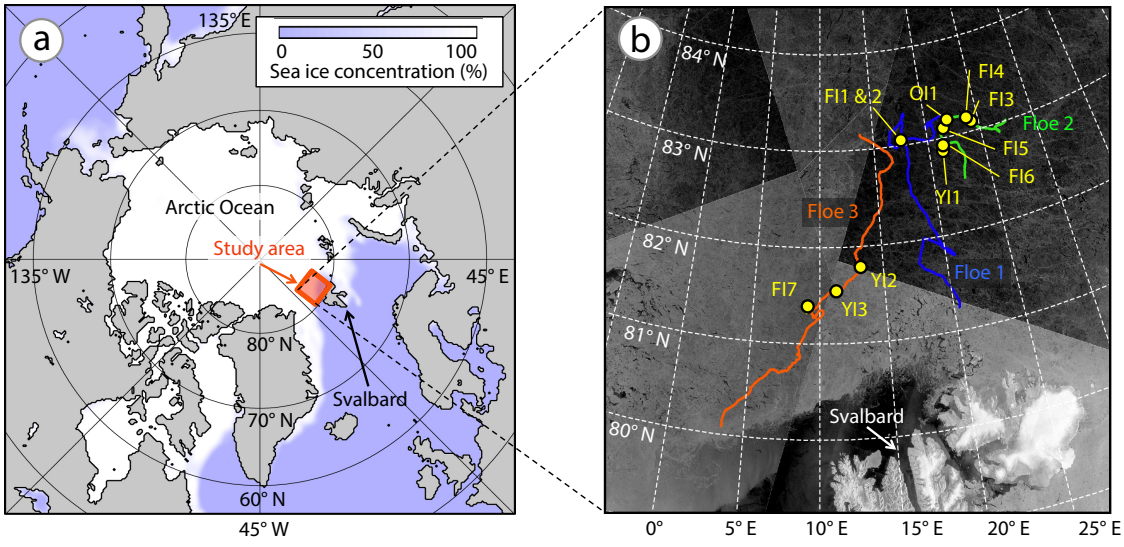


**Figure 1.** Location map of the sampling area north of Svalbard during N-ICE2015. Image of the sea ice concentrations **(a)** and station map **(b)** were derived from Special Sensor Microwave Imager (SSM/I) satellite data for mean of February 2015 and from Sentinel-1 (Synthetic Aperture Radar Sensor) satellite data, respectively.

**Table 1.** Station, date for $CO_2$ flux measurement, position, floe number, surface condition, ice type and thickness of snow, frost flowers, and sea ice.

| Station | Position | Date of 2015 | Floe number | Surface condition | Ice type[c] | Thickness (cm) | | |
|---|---|---|---|---|---|---|---|---|
| | | | | | | Snow | Frost flower | Sea ice |
| FI1 | 83°03.77 N, 17°34.94 E | 28 Jan | 1 | Frost flower | First-year ice | 0.0 | 1.0 | 37.0 |
| FI2 | 83°03.77 N, 17°34.94 E | 28 Jan | 1 | Snow | First-year ice | 8.0 | No | 35.0 |
| FI3 | 83°08.00 N, 24°09.02 E | 5 and 8 Mar[a] | 2 | Snow | First-year ice | 29.0 | No | 98.0 |
| FI4 | 83°10.56 N, 22°09.42 E | 9 Mar | 2 | Snow | First-year ice | 36.0 | No | 92.0 |
| FI5 | 83°06.02 N, 21°38.29 E | 10 and 11 Mar[b] | 2 | Snow | First-year ice | 3.0 | No | 48.0 |
| FI6 | 82°55.36 N, 21°25.92 E | 12 Mar | 2 | Snow | First-year ice | 37.0 | No | 69.0 |
| FI7 | 81°22.18 N, 08°59.93 E | 13 May | 3 | Snow | First-year ice | 26.5 | No | 127.0 |
| YI1 | 82°52.52 N, 21°16.54 E | 13 Mar | 2 | Frost flower | Young ice | 0.0 | 1.0 | 15.0 |
| YI2 | 81°46.53 N, 13°16.00 E | 5 May | 3 | Snow and frost flower mixed | Young ice | 2.5 | 2.5 | 17.5 |
| YI3 | 81°32.45 N, 11°17.20 E | 9 May | 3 | Snow and frost flower mixed | Young ice | 2.0 | 2.0 | 22.0 |
| OI1 | 83°07.18 N, 24°25.59 E | 6 Mar | 2 | Snow | Old ice (multi-year ice) | 60.0 | No | > 200 |

[a] Sea ice coring, brine, and snow sampling was conducted on 5 March 2015. [b] Sea ice coring, brine, and snow sampling was conducted on 10 March 2015.
[c] Ice type was categorized based on WMO (1970).

Formation of leads and their rapid refreezing provided us the opportunity to examine air–sea ice $CO_2$ fluxes over thin sea ice, occasionally covered with frost flowers at station YI1 (Fig. 2 and Table 1). Air temperature and wind speed were measured at a 10 m weather mast on the ice floe installed about 400 m away from R/V *Lance* (Cohen et al., 2017).

## 2.2 $CO_2$ flux measurements

The air–sea ice $CO_2$ flux was measured with LI-COR 8100-104 chambers connected to a LI-8100A soil $CO_2$ flux system (LI-COR Inc., USA) (Fig. 2). This enclosed chamber method has been widely applied over snow and sea ice (e.g., Schindlbacher et al., 2007; Geilfus et al., 2015). Two chambers were connected in a closed loop to the infrared gas analyzer (LI-8100A, LI-COR Inc., USA) to measure $CO_2$ concentration through the multiplexer (LI-8150, LI-COR Inc., USA) with an air pump rate at 3 L $min^{-1}$. Power was supplied by a car battery (8012-254, Optima Batteries Inc., USA). Four $CO_2$ standards (324–406 ppmv) traceable to the WMO scale (Inoue and Ishii, 2005) were prepared to calibrate the $CO_2$ gas analyzer prior to the observations. $CO_2$ flux was measured in the morning or in the afternoon during low-wind conditions (Table 2), to minimize the effect of wind on the flux (Bain et al., 2005).

One chamber was installed over undisturbed snow or frost flowers on the ice surface. The chamber collar was inserted 5 cm into the snow and 1 cm into ice at the frost flower site to avoid air leaks between the inside and outside of the chamber. The second chamber was installed on bulk sea ice af-

**Figure 2.** Photographs of the $CO_2$ flux chamber system at station YI1 north of Svalbard on 13 March 2015. $CO_2$ flux chamber was installed over the frost flowers on the new thin ice in the refreezing lead.

ter removing the snow or frost flowers. Flux measurements were begun immediately in order to minimize the changes of the ice surface condition. In order to evaluate the effect of removing snow on the ice surface temperature, temperature was monitored during $CO_2$ flux measurements at station FI6. A temperature sensor (RTR 52, T & D Corp., Japan) was installed in the top of the ice (1 cm) surface after snow removal. During the first $CO_2$ flux measurements (about 30 min), the ice surface temperature was stable at −5.8 °C, suggesting that the effect of removing snow on the variation of sea ice surface temperature was negligible within 30 min. The ice surface temperature decreased from −5.8 to −8.0 °C at 200 min after removal of snow. Therefore, in this paper, the data of the initial 30 min of $CO_2$ flux measurement after removal of snow or frost flowers were used. The chamber was closed for 20 min in a sequence. The 20 min time period was used because $CO_2$ fluxes over sea ice are much smaller than over land. The $CO_2$ concentrations within the chamber were monitored to ensure that they changed linearly throughout the measurement period (example given in Fig. 3). The $CO_2$ flux (mmol C m$^{-2}$ day$^{-1}$) (positive value indicates $CO_2$ being released from ice surface to air) was calculated based on the changes of the $CO_2$ concentration within the headspace of the chamber with LI-COR software (model: LI8100PC Client v.3.0.1.). The mean coefficient of variation for $CO_2$ flux measurements was less than 3.0 % for $CO_2$ flux values larger than ±0.1 mmol C m$^{-2}$ day$^{-1}$. For $CO_2$ flux values smaller than ±0.1 mmol C m$^{-2}$ day$^{-1}$, the mean coefficient of variation for $CO_2$ flux measurements was higher than 3.0 %, suggesting that the detection limit of this system is about 0.1 mmol C m$^{-2}$ day$^{-1}$.

**Table 2.** Station, snow density and water equivalent, brine volume fraction and temperature for sea ice (top 20 cm), brine temperature, salinity, dissolved inorganic carbon (DIC), total alkalinity (TA), $pCO_2$ ($pCO_{2b}$), and atmospheric temperature, wind speed, $pCO_2$ ($pCO_{2a}$)[a] and $\Delta\, pCO_{2b-a}$.

| Station | Snow | | Sea ice (top 20 cm) | | Brine | | | | | Atmosphere | | |
|---|---|---|---|---|---|---|---|---|---|---|---|---|
| | Density[b] (kg m$^{-3}$) | Water equivalent (kg m$^{-2}$) | Brine volume fraction (%) | Temperature (°C) (range) | Temperature (°C) | Salinity (μmol kg$^{-1}$) | DIC (μatm) | TA (μatm) | $pCO_{2b}$ (°C) | Temperature (m s$^{-1}$) | Wind speed (μatm) | $pCO_{2a}$ (μatm) | $\Delta\, pCO_{2b-a}$ |
| FI1 | _[c] | _[c] | _[c] | _[c] | _[c] | _[c] | _[c] | _[c] | _[c] | −31.6 | 4.0 | 405 | _[c] |
| FI2 | _[c] | _[c] | _[c] | _[c] | _[c] | _[c] | _[c] | _[c] | _[c] | −31.6 | 4.0 | 405 | _[c] |
| FI3 | 399 | 104 | 9 | −6.8 (−7.4 to −6.3) | −5.2 | 84.8 | 4628 | 5539 | 427 | −3.3 | 9.0 | 400 | 27 |
| FI4 | 400 | 180 | 9 | −4.7 (−5.5 to −3.7) | −5.3 | 86.6 | 4433 | 5490 | 334 | −3.5 | 6.2 | 386 | −52 |
| FI5 | 268 | 11 | 17 | −3.5 (−3.8 to −3.1) | −3.3 | 51.8 | 3261 | 3518 | 472 | −18.1 | 6.8 | 389 | 83 |
| FI6 | 343 | 127 | 13 | −4.8 (−5.7 to −3.8) | −4.8 | 84.0 | 4841 | 5493 | 693 | −25.0 | 3.6 | 400 | 293 |
| FI7 | _[c] | _[c] | _[c] | −6.1 (−6.1 to −5.8) | _[c] | _[c] | _[c] | _[c] | _[c] | −13.0 | 5.8 | 405 | _[c] |
| YI1 | _[c] | _[c] | 17 | −6.6 (−12.3 to −2.6) | _[c] | _[c] | _[c] | _[c] | _[c] | −26.0 | 2.6 | 402 | _[c] |
| YI2 | _[c] | _[c] | _[c] | −3.6 (−5.1 to −1.8) | _[c] | _[c] | _[c] | _[c] | _[c] | −16.2 | 4.5 | 407 | _[c] |
| YI3 | _[c] | _[c] | _[c] | −3.9 (−6.4 to −2.0) | _[c] | _[c] | _[c] | _[c] | _[c] | −14.2 | 6.7 | 410 | _[c] |
| OI1 | _[c] | _[c] | 0 | −10.8 (−11.0 to −10.9) | _[c] | _[c] | _[c] | _[c] | _[c] | −13.5 | 4.7 | 397 | _[c] |

[a] $pCO_{2a}$ (μatm) was calculated from $CO_2$ concentration (ppmv) at Ny-Ålesund, Svalbard (http://www.esrl.noaa.gov/gmd/dv/iadv/), taking into account the saturated water vapor and atmospheric pressures at sampling day. [b] Mean values for column. [c] "_" indicates no data. Due to logistical constraints, data of snow, sea ice, and brine were not obtained.

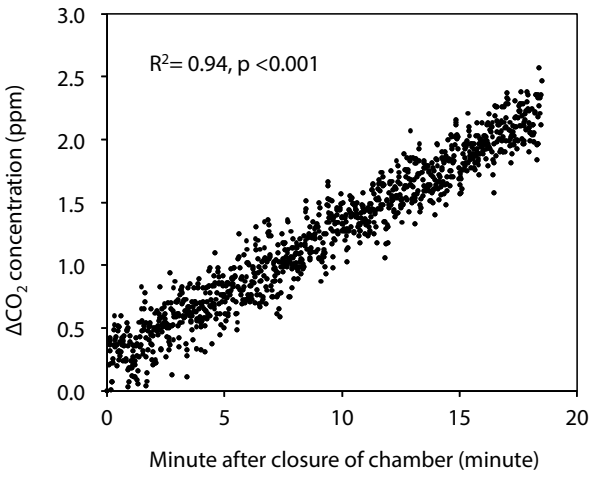


**Figure 3.** Example of the temporal variation in $CO_2$ concentration ($\Delta CO_2$) in the chambers installed at station YI1 that is use to calculate the $CO_2$ flux. $\Delta CO_2$ indicates the change in $CO_2$ concentration inside the chamber since the chamber was closed.

In this paper, we express the $CO_2$ flux measured over the snow and frost flowers as $F_{snow}$, and $F_{ff}$, respectively. The flux measured directly over the sea ice surface either on snow-free ice or after removal of snow and frost flowers as $F_{ice}$. $F_{snow}$ and $F_{ff}$ are the natural flux (snow and frost flowers are part of the natural system), and $F_{ice}$ is the potential flux in cases when snow or frost flowers are removed. While removal of snow and frost flowers is an artificial situation, comparisons between $F_{ice}$ and $F_{snow}$ or $F_{ff}$ provide information about the effect of snow and frost flowers on the $CO_2$ flux. Therefore, in this study, we examine both situations for $CO_2$ flux.

### 2.3 Sampling of snow, frost flowers, brine, and sea ice

For salinity measurements, separate samples were taken for snow only, snow and frost flowers, and sea ice surface scrapes. The samples were taken using a plastic shovel, placed into plastic bags and stored in an insulated box for transport to the ship lab for further processing. Samples were melted slowly (2–3 days) in the dark at +4 °C. The temperature of the snow and frost flower samples was measured during $CO_2$ flux measurements (approximately 60 min after the onset of the $CO_2$ flux measurement) using a needle-type temperature sensor (Testo 110 NTC, Brandt Instruments, Inc., USA). The accuracy of this sensor is ±0.2 °C. Snow density was obtained using a fixed volume sampler (Climate Engineering, Japan) and weight measurement. The depth of the snow pack and frost flowers was also recorded using a ruler.

Brine was also collected at stations FI3–6 for salinity, dissolved inorganic carbon (DIC), and total alkalinity (TA) measurements. Brine was collected from sack holes as described in Gleitz et al. (1995). The sack holes were drilled using a 9 cm diameter ice corer (Mark II coring system, Kovacs Enterprises, Inc., USA) to a depth of 30 cm. The sack holes were then covered with a lid of 5 cm thick urethane to reduce heat and gas transfer between brine and atmosphere. When brine accumulated at the bottom of the sack holes (approximately 15 min), it was collected with a plastic syringe (AS ONE Corporation, Japan) and kept in 500 mL unbreakable plastic bottles (I-Boy, AS ONE Corporation, Japan) in order to facilitate safe transport to the sampling sites in cold and harsh conditions. The brine bottles were filled without head space and immediately stored in an insulated box to prevent freezing. Immediately after returning to the ship, the brine samples were transferred to 250 mL borosilicate bottles (DURAN Group GmbH, Germany) for DIC and TA measurements using tubing to prevent contact with air. The samples were preserved with saturated mercuric chloride ($HgCl_2$, 60 µL for a 250 mL sample) and stored in the dark at +10 °C until analyses were performed at the Institute of Marine Research, Norway.

Sea ice was collected by the same ice corer as described for brine collection and at the same location as snow and frost flowers were collected. Sea ice temperature was measured by the same sensor as described for snow. For the ice cores, the temperature sensor was inserted in small holes drilled into the core. The core was then cut with a stainless steel saw into 10 cm sections and stored in plastic bags for subsequent salinity measurements. The ice core sections were kept at +4 °C and melted in the dark prior to measurement.

### 2.4 Sample analysis

Salinities for melted snow, frost flowers, sea ice, and brine were measured with a conductivity sensor (Cond 315i, WTW GmbH, Germany). For calibration of salinity measurement, a Guildline PORTASAL salinometer model 8410A, standardized by International Association for the Physical Sciences of the Oceans (IAPSO) standard seawater (Ocean Scientific International Ltd, UK), was used. The accuracy of this sensor was ±0.003.

Analytical methods for DIC and TA determination are fully described in Dickson et al. (2007). DIC in brine was determined using gas extraction of acidified sample followed by coulometric titration and photometric detection using a Versatile INstrument for the Determination of Total inorganic carbon and titration Alkalinity (VINDTA 3C, Germany). TA of brine was determined by potentiometric titration of 40 mL sample in open cell with 0.05 N hydrochloric acid using a Titrino system (Metrohm, Switzerland). The average SD for DIC and TA, determined from replicate sample analyses from one sample, was within ±2 µmol kg$^{-1}$ for both DIC and TA. The accuracy of the DIC and TA measurements were ±2 µmol kg$^{-1}$ for both DIC and TA, as estimated using Certified Reference Materials (CRM, provided by A. G. Dickson, Scripps Institution of Oceanography, USA). The $pCO_2$ of brine ($pCO_{2\,b}$) was derived from in situ tempera-

ture, salinity, DIC, and TA of brine using the carbonate speciation program CO2SYS (Pierrot et al., 2006). The calculated $pCO_{2\,b}$ values (Table 2) varied within 1.7 % when DIC and TA values were changed within the SD ($\pm 2\,\mu mol\,kg^{-1}$). We used the carbonate dissociation constants ($K_1$ and $K_2$) of Mehrbach et al. (1973) as refit by Dickson and Millero (1987) and the $KSO_4$ determined by Dickson (1990). The conditional stability constants used to derive $pCO_2$ are only valid for temperatures above 0 °C and salinities between 5 and 50. Studies in spring ice indicated that seawater thermodynamic relationships may be acceptable in warm and low-salinity sea ice (Delille et al., 2007). In sea ice brine at even moderate brine salinities of 80, Brown et al. (2014) found that measured and calculated values of the $CO_2$ system parameters can differ by as much as 40 %. However, because the $CO_2$ system parameters are much more variable in sea ice than in seawater, sea ice measurements demand less precision than those in seawater. Fransson et al. (2015) performed one of the few detailed analyses of the internal consistency using four sets of dissociation constants and found that the deviation between measured and calculated DIC varied between ±6 and ±11 $\mu mol\,kg^{-1}$, respectively. This error in calculated DIC was considered insignificant in relation to the natural variability in sea ice.

The $pCO_2$ of atmosphere was calculated from $CO_2$ concentration (ppmv) at Ny-Ålesund, Svalbard (https://www.esrl.noaa.gov/gmd/dv/iadv/graph.php?code=ZEP&program=ccgg&type=sc, last access: 2 June 2018), taking into account saturated water vapor and atmospheric pressure during sampling day.

The water equivalent was computed for snow by multiplying snow thickness by snow density (Jonas et al., 2009). Brine volume of sea ice was calculated from the temperature and salinity of sea ice according to Cox and Weeks (1983) and Petrich and Eicken (2010).

## 3 Results

### 3.1 Air temperature

Air temperature is shown in Fig. 4. During the study period, the air temperature varied considerably from a low of −41.3 °C (30 January) to a high of +1.7 °C (15 June) (Hudson et al., 2015). Even in wintertime (from January to March), rapid increases of air temperature from less than −30 up to −0.2 °C (e.g., 18 February) were observed. In springtime (from April to June) the air temperature increased continuously, and from 1 June air temperatures were near 0 °C, although rapid increases (and subsequent decreases) of air temperature to near 0 °C were observed on two occasions in mid-May (Cohen et al., 2017).

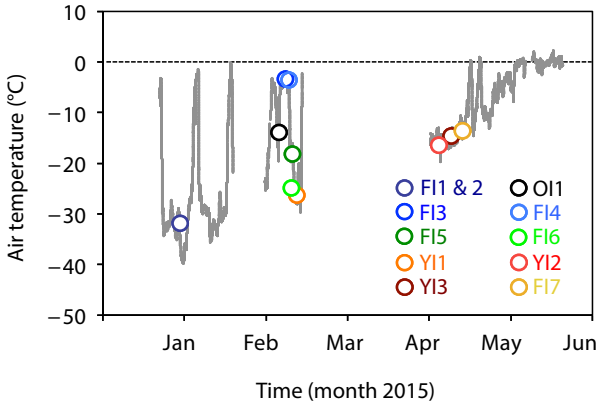


**Figure 4.** Time series of air temperature measured at the weather mast over the ice floe (10 m height) (Hudson et al., 2015). Blank period indicates no data. Colored symbols indicate the date for the chamber flux measurements. The horizontal dashed line indicates air temperature of 0 °C.

### 3.2 Characteristics of snow, sea ice, and frost flowers

The snow and ice thickness at the observation sites ranged between 0.0 and 60.0 cm and between 15.0 and > 200 cm, respectively (Table 1). The thin snow and ice represent newly formed ice in leads at station YI1. The thickness of the frost flowers ranged from 1.0 to 2.5 cm.

Figure 5 shows vertical profiles of snow and ice temperature and salinity in the top 20 cm of ice. Temperatures within the snowpack depended on the air temperature at the time of observation. However, the bottom of the snow and the surface of the sea ice were relatively warm ($T > -7.5$ °C), except for the frost flower station YI1 and the multi-year ice station OI1 (Fig. 5a and Table 2). High salinities ($S > 18.6$) characterized the bottom of the snow and the surface of the sea ice, except for the multi-year ice station OI1 (Fig. 5b). At the multi-year ice station OI1, salinity was zero through the snow and top of sea ice. Salinity of frost flowers was up to 92.8 for the thin ice station YI1 (Fig. 5b). Snow density and water equivalent ranged from 268 to 400 $kg\,m^{-3}$ and 11 to 180 $kg\,m^{-2}$, respectively (Table 2).

### 3.3 Physical and chemical properties of brine

The brine volume fraction, temperature, salinity, DIC, TA, and calculated $pCO_2$ are summarized in Table 2. Brine volume fraction in the top 20 cm of ice was between 9 to 17 %, except for the value of 0 % at the multi-year ice station OI1 (Table 2). Brine temperatures and salinity ranged from −5.3 to −3.3 °C and 51.8 to 86.6, respectively. DIC and TA of brine ranged from 3261 to 4841 $\mu mol\,kg^{-1}$ and 3518 to 5539 $\mu mol\,kg^{-1}$, respectively. The $pCO_2$ of brine ($pCO_{2\,b}$) (334–693 µatm) was generally higher than that of atmosphere ($pCO_{2\,a}$) (401 ± 7 µatm), except for station FI4.

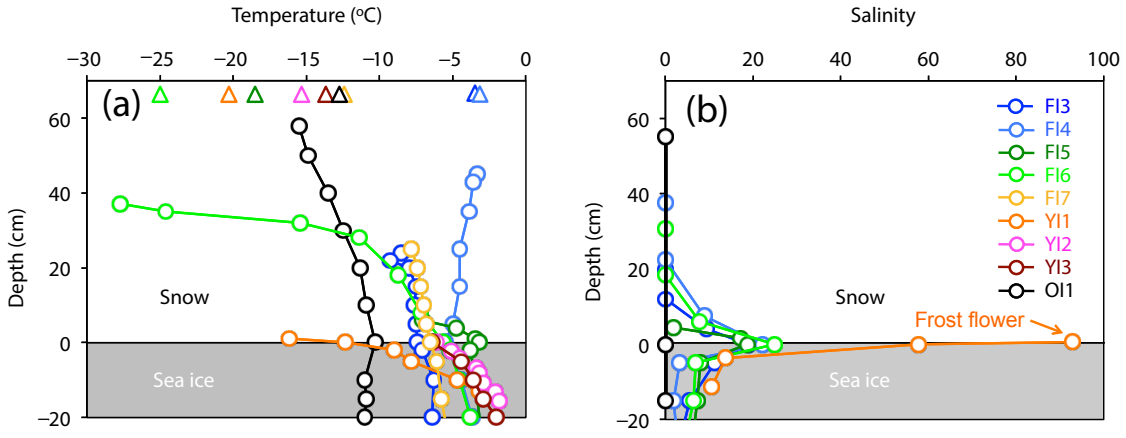


**Figure 5.** Vertical profiles of temperature **(a)** and salinity **(b)** in snow and sea ice (top 20 cm). The horizontal line indicates snow–ice interface. Shaded area indicates sea ice. The triangle in panel **(a)** indicates the air temperature for each station. For stations FI7 and YI2 and 3, we have no salinity data.

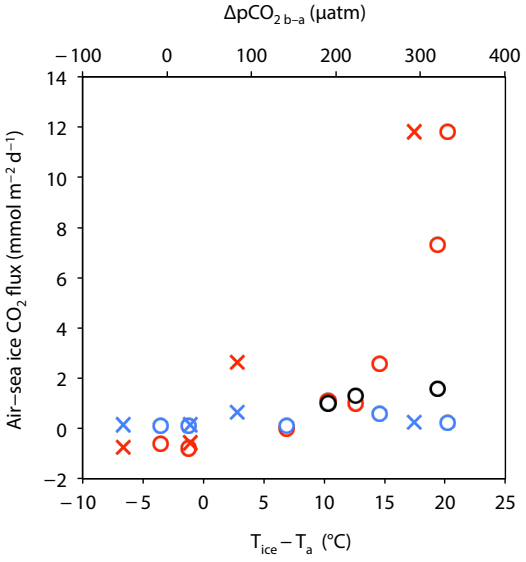


**Figure 6.** Relationships between mean air–sea ice $CO_2$ fluxes and temperature difference ($T_{ice}$–$T_a$) between ice (top 20 cm) ($T_{ice}$) and atmosphere ($T_a$) (circle) for $F_{snow}$ (blue), $F_{ff}$ (black), and $F_{ice}$ (red) for young and first-year sea ice. Relationships between mean air–sea ice $CO_2$ fluxes and the difference of $pCO_2$ ($\Delta\, pCO_{2\,b-a}$) between brine ($pCO_{2\,b}$) and atmosphere ($pCO_{2\,a}$) (cross) for $F_{snow}$ (blue) and $F_{ice}$ (red).

### 3.4 $CO_2$ flux

Table 3 summarizes the $CO_2$ flux measurements for each surface condition. For undisturbed natural surface conditions, i.e., measurements directly on the snow surface ($F_{snow}$) or the frost flowers ($F_{ff}$) on young ice, the mean $CO_2$ flux was $+0.2 \pm 0.2\,mmol\,C\,m^{-2}\,day^{-1}$ for $F_{snow}$ and $+1.0 \pm 0.6\,mmol\,C\,m^{-2}\,day^{-1}$ for $F_{ff}$. The potential flux in cases when snow or frost flowers had been removed ($F_{ice}$) was $+2.5 \pm 4.3\,mmol\,C\,m^{-2}\,day^{-1}$. The air–sea ice $CO_2$ fluxes measured over the ice surface ($F_{ice}$) increased with increasing differences in $pCO_2$ between brine and atmosphere ($\Delta\, pCO_{2\,b-a}$) with significant correlation ($R^2 = 0.9$, $p < 0.02$), but this was not the case for $F_{snow}$ ($R^2 = 0.0$, $p < 0.96$) (Fig. 6).

## 4 Discussion

### 4.1 Effect of snow cover on the physical properties of sea ice surface

In this study, we examined $CO_2$ fluxes between the sea ice and atmosphere in a wide range of air temperatures and diverse snow and ice conditions (Table 2). The bottom of the snow pack and the surface of the sea ice remained relatively warm ($> -7.5\,°C$) (Fig. 5a, Table 2), except for stations OI1 and YI1, even though air temperature was sometimes below $-40\,°C$ (Fig. 4). Relatively warm ice temperatures were likely due to the upward heat transport from the bottom of the ice and in some cases the thick insulating snow cover, except for stations OI1 and YI1 (Table 2). Therefore, snow acted as thermal insulator over sea ice, and in general the snow depths observed during N-ICE2015 point towards this being representative for first-year and second-year or older ice in the study region in winter 2015 (Rösel et al., 2018). The young and first-year ice surfaces were characterized by high salinities (Fig. 5b). During sea ice formation, upward brine transport to the snow pack occurs (e.g., Toyota et al., 2011). In addition, brine within the sea ice was not completely drained as compared to that of multi-year ice. Furthermore, formation of frost flowers and subsequent wicking up of surface brine into the frost flowers also provides high salinity at the surface of sea ice (Kaleschke et al., 2004; Geil-

**Table 3.** $CO_2$ flux measured over the snow ($F_{snow}$), frost flowers ($F_{ff}$) and ice surface ($F_{ice}$). Natural flux was emphasized as bold.

| Station | $CO_2$ flux (mmol C $m^{-2}$ $day^{-1}$) | | |
|---|---|---|---|
| | Natural flux (mean ± 1 SD) | | Potential flux |
| | $F_{snow}$ | $F_{ff}$ | $F^{a}_{ice}$ |
| FI1 | –[b] | **+0.1 ± 0.1** ($n = 7$)[c] | –[b] |
| FI2 | **+0.4 ± 0.3** ($n = 13$)[c] | –[b] | –[b] |
| FI3 | **+0.1 ± 0.1** ($n = 7$)[c] | –[b] | −0.6 |
| FI4 | **+0.1 ± 0.1** ($n = 6$)[c] | –[b] | −0.8 |
| FI5 | **+0.6 ± 0.3** ($n = 5$)[c] | –[b] | +2.6 |
| FI6 | **+0.2 ± 0.1** ($n = 5$)[c] | –[b] | +11.8 |
| FI7 | **+0.1 ± 0.1** ($n = 10$)[c] | –[b] | ±0.0 |
| YI1 | –[b] | **+1.6 ± 0.2** ($n = 6$)[c] | +7.3 |
| YI2 | –[b] | **+1.3 ± 0.2** ($n = 9$)[c] | +1.0 |
| YI3 | –[b] | **+1.0 ± 0.4** ($n = 8$)[c] | +1.1 |
| OI1 | **+0.1 ± 0.0** ($n = 6$)[c] | –[b] | +0.2 |
| Mean[d] | **+0.2 ± 0.2** ($n = 46$)[c] | **+1.0 ± 0.6** ($n = 30$)[c] | +2.5 ± 4.3 ($n = 9$)[c] |

[a] Data of first measurement after removal of snow or frost flower. [b] "–" indicates no data. [c] Number of measurements in bracket. [d] Data of station OI1 were not included.

fus et al., 2013; Barber et al., 2014; Fransson et al., 2015) as observed in this study ($S > 92$) (Fig. 5b). Snowfall over the frost flowers would have preserved the high salinity at the bottom of snow pack and top of sea ice for young and first-year ice.

As a result of the combination of the relatively high temperature and high salinity at the top of sea ice, brine volume fractions in the upper parts of the sea ice were high, up to 17 % (Table 2). It has been shown that ice permeability increases by an order of magnitude when brine volume fraction is greater than 5 % as compared to when the brine volume fraction is less than 5 % (Golden et al., 1998; Pringle et al., 2009; Zhou et al., 2013). A brine volume fraction of 5 % would correspond to a temperature of −5 °C for a bulk ice salinity of 5 – the so-called "law of fives" (Golden et al., 1998). Because sea ice temperatures are low, thereby reducing the permeability in winter season, air–sea ice $CO_2$ flux is generally at its minimum in the winter (e.g., Delille et al., 2014). However, in our study, the brine volume fractions were generally > 9 %, except for station OI1 with fresh ice at the surface, providing conditions for active gas exchange within sea ice and between sea ice and atmosphere. This situation was likely made possible due to the thick snow cover and relatively thin and young sea ice.

### 4.2 $CO_2$ fluxes over different sea ice surface types

The $CO_2$ flux measurements over different surface conditions indicate that the snow cover over sea ice affects the magnitude of air–sea ice $CO_2$ flux, especially for stations FI5 and FI6 (Table 3). For undisturbed natural surface conditions, the $CO_2$ flux measured directly over snow-covered first-year ice and young ice with frost flowers ($F_{snow}$ and $F_{ff}$) was lower in magnitude than that for potential flux obtained directly over the ice surface after removing snow ($F_{ice}$) for stations FI5, FI6, and YI1.

$F_{ff}$ indicates that the frost flower surface on young thin ice is a $CO_2$ source to the atmosphere and $F_{ff}$ was higher than $F_{snow}$, except for station FI1. This finding was consistent with the previous studies (Geilfus et al., 2013; Barber et al., 2014; Fransson et al., 2015). At multi-year ice station OI1, neither snow or ice surface acted as a $CO_2$ source/sink. The surface of multi-year ice did not contain any brine (Fig. 5b and Table 2), and the top of the ice was clear, colorless, and very hard, suggesting superimposed formation at the top of sea ice. This situation would be similar as for freshwater ice and superimposed ice as these non-porous media block gas exchange effectively at the sea ice surface (Delille et al., 2014). Snow ice and superimposed ice were frequently found in second-year ice cores during N-ICE2015 (Granskog et al., 2017), so the "blocking" of gas exchange in second-year and multi-year ice may be a widespread process in the Arctic.

The magnitude of positive $F_{snow}$ is less than $F_{ice}$ for stations FI5 and FI6 (Table 3), indicating that the potential $CO_2$ flux from sea ice decreased due to the presence of snow. Previous studies have shown that snow accumulation over sea ice effectively impedes $CO_2$ exchange (Nomura et al., 2013; Brown et al., 2015). Nomura et al. (2013) reported that 50–90 % of the potential $CO_2$ flux was reduced due to the presence of snow/superimposed ice at the water equivalent of 57–400 kg $m^{-2}$, indicating that the snow properties are an important factor that controls the $CO_2$ exchange through a snowpack. Comparisons between stations FI5 and FI6 for $F_{snow}/F_{ice}$ ratio (0.23 for FI5 and 0.02 for FI6) and water equivalent (11 kg $m^{-2}$ for FI5 and 127 kg $m^{-2}$ for FI6) indicate that the potential $CO_2$ flux is reduced (80 % for FI5

and 98 % for FI6 of the potential $CO_2$ flux) with increasing water equivalent. Although the magnitude of the potential $CO_2$ flux through the sea ice surface decreased by the presence of snow for stations FI5 and FI6 (Table 3), the snow surface still presents a $CO_2$ source to the atmosphere for low snow density and shallow depth conditions (e.g., $+0.6\,\mathrm{mmol\,C\,m^{-2}\,day^{-1}}$ for FI5).

For $F_{\mathrm{ice}}$, there were negative $CO_2$ fluxes at stations FI3 and FI4 ($-0.6\,\mathrm{mmol\,C\,m^{-2}\,day^{-1}}$ for FI3 and $-0.8\,\mathrm{mmol\,C\,m^{-2}\,day^{-1}}$ for FI4) (Table 3). These fluxes corresponded to low or negative $\Delta\,pCO_{2\,\mathrm{b-a}}$ (Table 2 and Fig. 6). Negative $CO_2$ fluxes should correspond to negative $\Delta\,pCO_{2\,\mathrm{b-a}}$. Therefore, the uncertainty for the calculation of carbonate chemistry may be one reason for the discrepancy in $pCO_2$ calculation at station FI3 (Brown et al., 2014).

### 4.3 Comparison to earlier studies on sea ice to air $CO_2$ flux

The $CO_2$ fluxes measured over the undisturbed natural surface conditions ($F_{\mathrm{snow}}$ and $F_{\mathrm{ff}}$) in this study ranged from $+0.1$ to $+1.6\,\mathrm{mmol\,C\,m^{-2}\,day^{-1}}$ (Table 3), which are at the lower end of the reported range based on the chamber method and eddy covariance method for natural and artificial sea ice ($-259.2$ to $+74.3\,\mathrm{mmol\,C\,m^{-2}\,day^{-1}}$) (Zemmelink et al., 2006; Nomura et al., 2006, 2010a, b, 2013; Miller et al., 2011; Papakyriakou and Miller, 2011; Geilfus et al., 2012, 2013, 2014; Barber et al., 2014; Delille et al., 2014; Sørensen et al., 2014; Brown et al., 2015; Kotovitch et al., 2016). Direct comparison to these previous studies is complicated because $CO_2$ flux measurements with both chamber and eddy covariance techniques were used during different conditions and ice surface characteristics. In addition, discrepancies between chamber and eddy covariance measurements of air–ice $CO_2$ fluxes have been repeatedly observed. The footprint size of $CO_2$ exchange measured with the two approaches (Zemmelink et al., 2006, 2008; Burba et al., 2008; Amiro, 2010; Miller et al., 2011, 2015; Papakyriakou and Miller, 2011; Sørensen et al., 2014) may be one reason for the large difference. The eddy covariance method reflects a flux integrated over a large area that can contain several different surface types. Therefore, eddy covariance appears to be more useful for understanding fluxes at large spatial and temporal scales. In contrast, the chamber method reflects the area where chamber was covered, and it is useful for understanding the relationship between fluxes and ice surface conditions on smaller scales. The different spatial scales of the two methods may therefore be one reason for the discrepancy in $CO_2$ flux measurements.

Comparison of the natural $CO_2$ flux range ($+0.1$ to $+1.6\,\mathrm{mmol\,C\,m^{-2}\,day^{-1}}$ for $F_{\mathrm{snow}}$ and $F_{\mathrm{ff}}$) (Table 3) with previous estimates derived from the chamber method ($-5.2$ to $+6.7\,\mathrm{mmol\,C\,m^{-2}\,day^{-1}}$) (Nomura et al., 2006, 2010a, b, 2013; Geilfus et al., 2012, 2013, 2014; Barber et al., 2014; Delille et al., 2014; Brown et al., 2015; Kotovitch et al., 2016) (these studies include both natural and potential fluxes) shows that $CO_2$ fluxes during the N-ICE2015 experiment are at the lower end of positive values. However, our potential $CO_2$ flux ($F_{\mathrm{ice}}$) was a larger $CO_2$ source (up to $+11.8\,\mathrm{mmol\,C\,m^{-2}\,day^{-1}}$) than reported in previous studies ($+6.7\,\mathrm{mmol\,C\,m^{-2}\,day^{-1}}$). In our study, the maximum potential flux ($+11.8\,\mathrm{mmol\,C\,m^{-2}\,day^{-1}}$) was obtained for $F_{\mathrm{ice}}$ at station FI6 (Table 3). In this situation, $\Delta\,pCO_{2\,\mathrm{b-a}}$ (293 µatm) was the highest (Table 2 and Fig. 6), and it is reasonable to consider this as the highest magnitude of positive $CO_2$ flux within our study. However, a previous study by closed chamber method showed that even for a similar $\Delta\,pCO_{2\,\mathrm{b-a}}$ (297 µatm) and brine volume fraction (10–15 %), the $CO_2$ flux was $+0.7\,\mathrm{mmol\,C\,m^{-2}\,day^{-1}}$ for artificial sea ice with no snow in the tank experiment (Nomura et al., 2006).

The $CO_2$ flux between the sea ice and overlying air can be expressed by the following equation:

$$F_{CO_2} = r_{\mathrm{b}} k \alpha \Delta pCO_{2\,\mathrm{b-a}},$$

where $r_{\mathrm{b}}$ is the ratio of surface of the brine channel to sea ice surface, and we assume that the value of $r_{\mathrm{b}}$ is equal to brine volume fraction, $k$ is the gas transfer velocity, $\alpha$ is the solubility of $CO_2$ (Weiss, 1974), and $\Delta\,pCO_{2\,\mathrm{b-a}}$ is the difference in $pCO_2$ between brine and atmosphere. The equation is based on the fact that $CO_2$ transfer between seawater and air is controlled by processes in the near-surface water (Liss, 1973). The gas transfer velocity ($k$) calculated from $F$, $r_{\mathrm{b}}$, $\alpha$, and $\Delta\,pCO_{2\,\mathrm{b-a}}$ was $5.12\,\mathrm{m\,day^{-1}}$ for $F_{\mathrm{ice}}$ at station FI6 and $0.29\,\mathrm{m\,day^{-1}}$ for the tank experiment examined in Nomura et al. (2006). This result clearly indicates that the gas transfer velocity for $F_{\mathrm{ice}}$ at station FI6 is higher than that of the tank experiment examined in Nomura et al. (2006) even with very similar $\Delta\,pCO_{2\,\mathrm{b-a}}$ and brine volume fraction.

Here, we surmise that the gas transfer velocity, and thereby $CO_2$ flux, is greatly enhanced by the temperature difference between sea ice surface and atmosphere. Previous studies indicate that there is an unstable air density gradient in a dry snowpack due to basal heating and the strong temperature difference develops between bottom and top of snow (e.g., Powers et al., 1985; Severinghaus et al., 2010), which enhances the flow of air through the snowpack. We propose that the mixing and transport of gas within the snowpack could also occur over sea ice. Because temperatures at the bottom of snow and the top of sea ice were relatively warm due to a thick insulating snow over sea ice, there was a strong temperature difference between sea ice surface and atmosphere when air temperature was low (Fig. 5a and Table 2). For station FI6, the temperature difference between the sea ice surface and atmosphere was 20.2 °C after snow removal. In contrast, in the tank experiment by Nomura et al. (2006), the temperature difference between sea ice surface (top 1.5 cm) and air in the headspace was only 4.5 °C.

Figure 6 shows the relationship between mean air–sea ice $CO_2$ fluxes and temperature difference between ice and at-

mosphere. The strong dependence of $CO_2$ flux with temperature difference ($T_{ice}$–$T_a$) was observed, especially for $F_{ff}$ and $F_{ice}$ ($R^2 > 0.7$, $p < 0.01$, linear fitting) (Fig. 6). Due to the high brine volume fractions (Table 2), the sea ice surface had enough permeability for gas exchange. In addition, ice temperatures were similar for young and first-year ice (Table 2), indicating that $pCO_2$ at the top of the sea ice and $CO_2$ flux would be of similar order of magnitude if thermodynamic processes dominated. Therefore, our results suggest that the $CO_2$ fluxes, even over the frost flowers as a natural condition, would be enhanced by the upward transport of air containing high $CO_2$ from the surface of sea ice to the atmosphere due to the strong temperature difference between sea ice surface and atmosphere. Although the presence of snow on sea ice has potential to produce a larger temperature difference between sea ice surface and atmosphere and promote the upward transport, the magnitude of the $CO_2$ flux decreased due to the presence of snow. However, for young sea ice with frost flowers (e.g., station YI1), ice surface temperature was warm (Table 2), suggesting that $CO_2$ flux would be enhanced by the large temperature difference between sea ice surface and atmosphere.

## 5 Conclusions

We measured $CO_2$ fluxes along with sea ice and snow physical and chemical properties over first-year and young sea ice north of Svalbard in the Arctic pack ice. Our results suggest that young thin snow-free ice, with or without frost flowers, is a source of atmospheric $CO_2$ due to the high $pCO_2$ and salinity and relatively high sea ice temperature. Although the potential $CO_2$ flux from the sea ice surface decreased due to the presence of snow, the snow surface still presents a modest $CO_2$ source to the atmosphere for low snow density and shallow depth situations. The highest ice-to-air fluxes were observed over thin young sea ice formed in leads. During N-ICE2015 the ice pack was dynamic, and formation of open water was associated with storms, where new ice was formed. The subsequent ice growth in these leads is especially important for the ice-to-air $CO_2$ fluxes in winter since the flux from young ice is an order of magnitude larger than from snow-covered first-year and older ice.

*Data availability.* Data used in this paper will be available at Norwegian Polar Data Centre (data.npolar.no).

*Competing interests.* The authors declare that they have no conflict of interest.

*Acknowledgements.* We would like to express heartfelt thanks to the crew of R/V *Lance* and all members of the N-ICE2015 expedition for their support in conducting the field work. This work was supported by the Japan Society for the Promotion of Science (15K16135, 24-4175), Research Council of Norway (KLIMAFORSK programme, grant 240639), the Centre of Ice, Climate and Ecosystems (ICE) at the Norwegian Polar Institute through the N-ICE project, the Ministry of Climate and Environment and the Ministry of Foreign Affairs of Norway, the Grant for Joint Research Program of the Institute of Low Temperature Science, Hokkaido University, and the Grant for Arctic Challenge for Sustainability. Agneta Fransson, Melissa Chierici, and Mats A. Granskog were supported by the flagship research program "Ocean acidification and ecosystem effects in Northern waters" within the FRAM-High North Research Centre for Climate and the Environment. Bruno Delille is a research associate of the F.R.S-FNRS.

Edited by: Paul Stoy
Reviewed by: Sian Henley and one anonymous referee

## References

Amiro, B.: Estimating annual carbon dioxide eddy fluxes using open-path analysers for cold forest sites, Agr. Forest Meteorol., 150, 1366–1372, 2010.

Bain, W. G., Hutyra, L., Patterson, D. C., Bright, A. V., Daube, B. C., Munger, J. W., and Wofsy, S. C.: Wind-induced error in the measurement of soil respiration using closed dynamic chambers, Agr. Forest Meteorol., 131, 225–232, 2005.

Barber, D. G., Ehn, J. K., Pućko, M., Rysgaard, S., Deming, J. W., Bowman, J. S., Papakyriakou, T., Galley, R. J., and Søgaard, D. H.: Frost flowers on young Arctic sea ice: the climatic, chemical and microbial significance of an emerging ice type, J. Geophys. Res.-Atmos., 119, 11593–11612, https://doi.org/10.1002/2014JD021736, 2014.

Bowling, D. R. and Massman, W. J.: Persistent wind-induced enhancement of diffusive $CO_2$ transport in a mountain forest snowpack, J. Geophys. Res., 116, G04006, https://doi.org/10.1029/2011JG001722, 2011.

Brown, K. A, Miller, L. A., Davelaar, M., Francois, R., and Tortell, P. D.: Over-determination of the carbonate system in natural sea ice brine and assessment of carbonic acid dissociation constants under low temperature, high salinity conditions, Mar. Chem., 165, 36–45, https://doi.org/10.1016/j.marchem.2014.07.005, 2014.

Brown, K. A., Miller, L. A., Mundy, C. J., Papakyriakou, T., Francois, R., Gosselin, M., Carnat, G., Swystun, K., and Tortell, P. D.: Inorganic carbon system dynamics in landfast Arctic sea ice during the early-melt period, J. Geophys. Res.-Oceans, 120, 3542–3566, https://doi.org/10.1002/2014JC010620, 2015.

Burba, G., McDermitt, D., Grelle, A., Anderson, D., and Xu, L.: Addressing the influence of instrument surface heat exchange on the measurements of $CO_2$ flux from open-path gas analyzers, Glob. Change Biol., 14, 1854–1876, 2008.

Cohen, L., Hudson, S. R., Walden, V. P., Graham, R. M., and Granskog, M. A.: Meteorological conditions in a thinner Arctic sea ice regime from winter through summer during the Norwegian young sea ICE expedition (N-ICE2015), J. Geophys. Res.-Atmos., 122, 7235–7259, https://doi.org/10.1002/2016JD026034, 2017.

Cox, G. F. N. and Weeks, W. F.: Equations for determining the gas and brine volumes in sea-ice samples, J. Glaciol., 29, 306–316, 1983.

Delille, B., Jourdain, B., Borges, A. V., Tison, J.-L., and Delille, D.: Biogas ($CO_2$, $O_2$, dimethylsulfide) dynamics in spring Antarctic fast ice, Limnol. Oceanogr., 52, 1367–1379, 2007.

Delille, B., Vancoppenolle, M., Geilfus, N.-X., Tilbrook, B., Lannuzel, D., Schoemann, V., Becquevort, S., Carnat, G., Delille, D., Lancelot, C., Chou, L., Dieckmann, G. S., and Tison, J.-L.: Southern Ocean $CO_2$ sink: the contribution of the sea ice, J. Geophys. Res.-Oceans, 119, 6340–6355, 2014.

Dickson, A. G.: Thermodynamics of the dissociation of boric acid in synthetic seawater from 273.15 to 318.15 K, Deep-Sea Res., 37, 755–766, 1990.

Dickson, A. G. and Millero, F. J.: A comparison of the equilibrium constants for the dissociation of carbonic acid in seawater media, Deep-Sea Res., 34, 1733–1743, 1987.

Dickson, A. G., Sabine, C. L., and Christian, J. R. (Eds.): Guide to Best Practices for Ocean $CO_2$ Measurements, PICES Special Publication, 3, 191 pp., 2007.

Fransson, A., Chierici, M., Miller, L. A., Carnat, G., Thomas, H., Shadwick, E., Pineault, S., and Papakyriakou, T. M.: Impact of sea ice processes on the carbonate system and ocean acidification state at the ice–water interface of the Amundsen Gulf, Arctic Ocean, J. Geophys. Res., 118, 1–23, https://doi.org/10.1002/2013JC009164, 2013.

Fransson, A., Chierici, M., Abrahamsson, K., Andersson, M., Granfors, A., Gårdfeldt, K., Torstensson, A., and Wulff, A.: $CO_2$-system development in young sea ice and $CO_2$ gas exchange at the ice/air interface mediated by brine and frost flowers in Kongsfjorden, Spitsbergen, Ann. Glaciol., 56, 69, https://doi.org/10.3189/2015AoG69A563, 2015.

Fransson, A., Chierici, M., Skjelvan, I., Olsen, A., Assmy, P., Peterson, A. K., and Ward, B.: Effects of sea-ice and biogeochemical processes and storms on under-ice water $fCO_2$ during the winter-spring transition in the high Arctic Ocean: implications for sea–air $CO_2$ fluxes, J. Geophys. Res.-Oceans, 122, 5566–5587, https://doi.org/10.1002/2016JC012478, 2017.

Geilfus, N.-X., Carnat, G., Papakyriakou, T., Tison, J.-L., Else, B., and co-authors: Dynamics of $pCO_2$ and related air–ice $CO_2$ fluxes in the Arctic coastal zone (Amundsen Gulf, Beaufort Sea), J. Geophys. Res., 117, C00G10, https://doi.org/10.1029/2011JC007118, 2012.

Geilfus, N.-X., Carnat, G., Dieckmann, G. S., Halden, N., Nehrke, G., and co-authors: First estimates of the contribution of $CaCO_3$ precipitation to the release of $CO_2$ to the atmosphere during young sea ice growth, J. Geophys. Res., 118, 244–255, https://doi.org/10.1029/2012JC007980, 2013.

Geilfus, N.-X., Tison, J.-L., Ackley, S. F., Galley, R. J., Rysgaard, S., Miller, L. A., and Delille, B.: Sea ice $pCO_2$ dynamics and air–ice $CO_2$ fluxes during the Sea Ice Mass Balance in the Antarctic (SIMBA) experiment – Bellingshausen Sea, Antarctica, The Cryosphere, 8, 2395–2407, https://doi.org/10.5194/tc-8-2395-2014, 2014.

Geilfus, N.-X., Galley, R. J., Crabeck, O., Papakyriakou, T., Landy, J., Tison, J.-L., and Rysgaard, S.: Inorganic carbon dynamics of melt-pond-covered first-year sea ice in the Canadian Arctic, Biogeosciences, 12, 2047–2061, https://doi.org/10.5194/bg-12-2047-2015, 2015.

Gleitz, M., Vonderlo, M. R., Tomas, D. N., Dieckmann, G. S., and Millero, F. J.: Comparison of summer and winter inorganic carbon, oxygen and nutrient concentrations in Antarctic sea ice brine, Mar. Chem., 51, 81–89, 1995.

Golden, K. M., Ackley, S. F., and Lytle, V. I.: The percolation phase transition in sea ice, Science, 282, 2238–2241, 1998.

Granskog, M. A., Assmy, P., Gerland, S., Spreen, G., Steen, H., and co-authors: Arctic research on thin ice: consequences of Arctic sea ice loss, EOS T. Am. Geophys. Un., 97, 22–26, https://doi.org/10.1029/2016EO044097, 2016.

Granskog, M. A., Rosel, A., Dodd, P. A., Divine, D., Gerland, S., Martma, T., and Leng M. J.: Snow contribution to first-year and second-year Arctic sea ice mass balance north of Svalbard, J. Geophys. Res.-Oceans, 122, 2539–2549, https://doi.org/10.1002/2016JC012398, 2017.

Hudson, S. R., Cohen, L., and Walden, V.: N-ICE2015 surface meteorology (Data set), Norwegian Polar Institute, https://doi.org/10.21334/npolar.2015.056a61d1, 2015.

Inoue, H. Y. and Ishii, M.: Variations and trends of $CO_2$ in the surface seawater in the Southern Ocean south of Australia between 1969 and 2002, Tellus B, 57, 58–69, 2005.

Jonas, T., Marty, C., and Magnusson, J.: Estimating the snow water equivalent from snow depth measurements in the Swiss Alps, J. Hydrol., 378, 161–167, 2009.

Kaleschke, L., Richter, A., Burrows, J., Afe, O., Heygster, G., and co-authors: Frost flowers on sea ice as a source of sea salt and their influence on tropospheric halogen chemistry, Geophys. Res. Lett., 31, L16114, https://doi.org/10.1029/2004GL020655, 2004.

Kotovitch, M., Moreau, S., Zhou, J., Vancoppenolle, M., Dieckmann, G. S., Evers, K.-U., Van der Linden, F., Thomas, D. N., Tison, J.-L., and Delille, B.: Air–ice carbon pathways inferred from a sea ice tank experiment, Elementa, 4, 112, https://doi.org/10.12952/journal.elementa.000112, 2016.

Lindsay, R. and Schweiger, A.: Arctic sea ice thickness loss determined using subsurface, aircraft, and satellite observations, The Cryosphere, 9, 269–283, https://doi.org/10.5194/tc-9-269-2015, 2015.

Liss, P. S.: Processes of gas exchange across an air–water interface, Deep-Sea Res., 20, 221–238, 1973.

Massman, W., Sommerfeld, R., Zeller, K., Hehn, T., Hudnell, L., and Rochelle, S.: $CO_2$ flux through a Wyoming seasonal snowpack: diffusional and pressure pumping effects, in: Biogeochemistry of Seasonally Snow-Covered Catchments, Proceedings of a Boulder Symposium, July 1995, IAHS Publ., 228, 71–79, 1995.

Massom, R. A., Eicken, H., Haas, C., Jeffries, M. O., Drinkwater, M. R., Sturm, M., Worby, A. P., Wu, X., Lytle, V. I., Ushio, S., Morris, K., Reid, P. A., Warren, S. G., and Allison I.: Snow on Antarctic sea ice, Rev. Geophys., 39, 413–445, 2001.

Mehrbach, C., Culberson, C. H., Hawley, J. E., and Pytkowicz, P. M.: Measurement of the apparent dissociation constant of carbonic acid in seawater at atmospheric pressure, Limnol. Oceanogr., 18, 897–907, 1973.

Meier, W. N., Hovelsrud, G. K., van Oort, B. E. H., Key, J. R., Kovacs, K. M., Michel, C., Haas, C., Granskog, M. A., Gerland, S., Perovich, D. K., Makshtas, A., and Reist, J. D.: Arctic sea ice in transformation: a review of recent observed changes and impacts on biology and human activity, Rev. Geophys., 52, 185–217, https://doi.org/10.1002/2013RG000431, 2014.

Merkouriadi, I., Gallet, J.-C., Graham, R. M., Liston, G. E., Polashenski, C., Rösel, A., and Gerland, S.: Winter snow conditions on Arctic sea ice north of Svalbard during the Norwegian young sea ICE (N-ICE2015) expedition, J. Geophys. Res.-Atmos., 122, 10837–10854, https://doi.org/10.1002/2017JD026753, 2017.

Miller, L. A., Papakyriakou, T. N., Collins, R. E., Deming, J. W., Ehn, J. K., Macdonald, R. W., Mucci, A., Owens, O., Raudsepp, M., and Sutherland, N.: Carbon dynamics in sea ice: a winter flux time series, J. Geophys. Res., 116, C02028, https://doi.org/10.1029/2009JC006058, 2011.

Miller, L. A., Fripiat, F., Else, B. G. T., Bowman, J. S., Brown, K. A., Collins, R. E., Ewert, M., Fransson, A., Gosselin, M., Lannuzel, D., Meiners, K. M., Michel, C., Nishioka, J., Nomura, D., Papadimitriou, S., Russell, L. M., Sørensen, L. L., Thomas, D. N., Tison, J.-L., van Leeuwe, M. A., Vancoppenolle, M., Wolff, E. W., and Zhou, J.: Methods for biogeochemical studies of sea ice: the state of the art, caveats, and recommendation, Elementa, 3, 000038, https://doi.org/10.12952/journal.elementa.000038, 2015.

Nomura, D., Inoue, H. Y., and Toyota, T.: The effect of sea-ice growth on air–sea $CO_2$ flux in a tank experiment, Tellus B, 58, 418–426, 2006.

Nomura, D., Inoue, H. Y., Toyota, T., and Shirasawa, K.: Effects of snow, snowmelting and refreezing processes on air–sea-ice $CO_2$ flux, J. Glaciol., 56, 196, 262–270, 2010a.

Nomura, D., Eicken, H., Gradinger, R., and Shirasawa, K.: Rapid physically driven inversion of the air–sea ice $CO_2$ flux in the seasonal landfast ice off Barrow, Alaska after onset of surface melt, Cont. Shelf Res., 30, 1998–2004, 2010b.

Nomura, D., Granskog, M. A., Assmy, P., Simizu, D., and Hashida, G.: Arctic and Antarctic sea ice acts as a sink for atmospheric $CO_2$ during periods of snow melt and surface flooding, J. Geophys. Res.-Oceans, 118, 6511–6524, 2013.

Papadimitriou, S., Kennedy, H., Norman, L., Kennedy, D. P., Dieckmann, G. S., and Thomas, D. N.: The effect of biological activity, $CaCO_3$ mineral dynamics, and $CO_2$ degassing in the inorganic carbon cycle in sea ice in late winter-early spring in the Weddell Sea, Antarctica, J. Geophys. Res., 117, C08011, https://doi.org/10.1029/2012JC008058, 2012.

Papakyriakou, T. and Miller, L. A.: Springtime $CO_2$ exchange over seasonal sea ice in the Canadian Arctic Archipelago, Ann. Glaciol., 52, 215–224, 2011.

Parmentier, F. J. W., Christensen, T. R., Sørensen, L. L., Rysgaard, S., McGuire, A. D., Miller, P. A., and Walker, D. A.: The impact of lower sea–ice extent on Arctic greenhouse-gas exchange, Nat. Clim. Change, 3, 195–202, https://doi.org/10.1038/nclimate1784, 2013.

Petrich, C. and Eicken, H.: Growth, structure and properties of sea ice, in: Sea Ice, edited by: Thomas, D. N. and Dieckmann, G. S., 2nd edn., Wiley–Blackwell, Oxford, 23–77, 2010.

Pierrot, D., Lewis, E., and Wallace, D. W. R.: MS Excel Program Developed for $CO_2$ System Calculations, ORNL/CDIAC-105a, Carbon Dioxide Information Analysis Center, Oak Ridge National Laboratory, U.S. Department of Energy, Oak Ridge, Tennessee, https://doi.org/10.3334/CDIAC/otg.CO2SYS_XLS_CDIAC105a, 2006.

Powers, D., Oneill, K., and Colbeck, S. C.: Theory of natural convection in snow, J. Geophys. Res.-Atmos., 90, 10641–10649, https://doi.org/10.1029/Jd090id06p10641, 1985.

Pringle, D. J., Miner, J. E., Eicken, H., and Golden, K. M.: Pore space percolation in sea ice single crystals, J. Geophys. Res., 114, C12017, https://doi.org/10.1029/2008JC005145, 2009.

Rysgaard, S., Søgaard, D. H., Cooper, M., Pućko, M., Lennert, K., Papakyriakou, T. N., Wang, F., Geilfus, N. X., Glud, R. N., Ehn, J., McGinnis, D. F., Attard, K., Sievers, J., Deming, J. W., and Barber, D.: Ikaite crystal distribution in winter sea ice and implications for $CO_2$ system dynamics, The Cryosphere, 7, 707–718, https://doi.org/10.5194/tc-7-707-2013, 2013.

Rösel, A., Itkin, P., King, J., Divine, D., Wang, C., Granskog, M. A., Krumpen, T., and Gerland, S.: Thin sea ice, thick snow, and widespread negative freeboard observed during N-ICE2015 north of Svalbard, J. Geophys. Res.-Oceans, 123, 1156–1176, https://doi.org/10.1002/2017JC012865, 2018.

Schindlbacher, A., Zechmeister-Boltenstern, S., Glatzel, G., and Jandl, R.: Winter soil respiration from an Austrian mountain forest, Agr. Forest Meteorol., 146, 205–215, https://doi.org/10.1016/j.agrformet.2007.06.001, 2007.

Severinghaus, J. P., Albert, M. R., Courville, Z. R., Fahnestock, M. A., Kawamura, K., Montzka, S. A., Mühle, J., Scambos, T. A., Shields E., Shuman, C. A., Suwa, M., Tans, T., and Weiss, R. F.: Deep air convection in the firn at a zero-accumulation site, central Antarctica, Earth Planet. Sc. Lett., 293, 359–367, https://doi.org/10.1016/J.Epsl.2010.03.003, 2010.

Stroeve, J. C., Serreze, M. C., Holland, M. M., Kay, J. E., Maslanik, J., and Barrett, A. P.: The Arctic's rapidly shrinking sea ice cover: a research synthesis, Climatic Change, 110, 1005, https://doi.org/10.1007/s10584-011-0101-1, 2012.

Sørensen, L. L., Jensen, B., Glud, R. N., McGinnis, D. F., Sejr, M. K., Sievers, J., Søgaard, D. H., Tison, J.-L., and Rysgaard, S.: Parameterization of atmosphere–surface exchange of $CO_2$ over sea ice, The Cryosphere, 8, 853–866, https://doi.org/10.5194/tc-8-853-2014, 2014.

Takagi, K., Nomura, M., Ashiya, D., Takahashi, H., Sasa, K., Fujinuma, Y., Shibata, H., Akibayashi, Y., and Koike, T.: Dynamic carbon dioxide exchange through snowpack by wind-driven mass transfer in a conifer-broadleaf mixed forest in northernmost Japan, Global Biogeochem. Cy., 19, GB2012, https://doi.org/10.1029/2004GB002272, 2005.

Toyota, T., Massom, R., Tateyama, K., Tamura, T., and Fraser, A.: Properties of snow overlying the sea ice off East Antarctica in late winter 2007, Deep-Sea Res. Pt. II, 58, 1137–1148, 2011.

Vancoppenolle, M., Meiners, K. M., Michel, C., Bopp, L., Brabant, F., Carnat, G., Delille, B., Lannuzel, D., Madec, G., Moreau, S., Tison, J.-L., and van der Merwe, P.: Role of sea ice in global biogeochemical cycles: emerging views and challenges, Quaternary Sci. Rev., 79, 207–230, 2013.

Weiss, R. F.: Carbon dioxide in water and seawater: the solubility of a non-ideal gas, Mar. Chem., 2, 203–215, 1974.

WMO: WMO sea-ice nomenclature, terminology, codes and illustrated glossary, WMO/OMM/BMO 259 TP. 145, with amendments by ETSI-I, Buenos-Aires, 2002, Secretariat of the World Meteorol. Org., Geneva, 1970.

Zemmelink, H. J., Delille, B., Tison, J.-L., Hintsa, E. J., Houghton, L., and Dacey, J. W. H.: $CO_2$ deposition over the multi-year ice

of the western Weddell Sea, Geophys. Res. Lett., 33, L13606, https://doi.org/10.1029/2006GL026320, 2006.

Zemmelink, H. J., Dacey, J. W. H., Houghton, L., Hintsa. E. J., and Liss, P. S.: Dimethylsulfide emissions over the multi-year ice of the western Weddell Sea, Geophys. Res. Lett., 35, L06603, https://doi.org/10.1029/2007GL031847, 2008.

Zhou, J., Delille, B., Eicken, H., Vancoppenolle, M., Brabant, F., Carnat, G., Geilfus, N.-X., Papakyriakou, T., Heinesch, B., and Tison J.-L.: Physical and biogeochemical properties in landfast sea ice (Barrow, Alaska): insights on brine and gas dynamics across seasons, J. Geophys. Res., 118, 3172–3189, 2013.